Biophysical Journal
Article

Biophysical Society

Assaying How Phagocytic Success Depends on the Elasticity of a Large Target Structure

Megan Davis-Fields,[1,2] Layla A. Bakhtiari,[2,3] Ziyang Lan,[4] Kristin N. Kovach,[2,3] Liyun Wang,[2,3] Elizabeth M. Cosgriff-Hernandez,[4] and Vernita D. Gordon[1,2,3,*]

[1]Institute for Cellular and Molecular Biology, [2]Center for Nonlinear Dynamics, [3]Department of Physics, and [4]Department of Biomedical Engineering, The University of Texas at Austin, Austin, Texas

ABSTRACT Biofilm infections can consist of bacterial aggregates that are an order of magnitude larger than neutrophils, phagocytic immune cells that densely surround aggregates but do not enter them. Because a neutrophil is too small to engulf the entire aggregate, it must be able to detach and engulf a few bacteria at a time if it is to use phagocytosis to clear the infection. Current research techniques do not provide a method for determining how the success of phagocytosis, here defined as the complete engulfment of a piece of foreign material, depends on the mechanical properties of a larger object from which the piece must be removed before being engulfed. This article presents a step toward such a method. By varying polymer concentration or cross-linking density, the elastic moduli of centimeter-sized gels are varied over the range that was previously measured for *Pseudomonas aeruginosa* biofilms grown from clinical bacterial isolates. Human neutrophils are isolated from blood freshly drawn from healthy adult volunteers, exposed to gel containing embedded beads for 1 h, and removed from the gel. The percentage of collected neutrophils that contain beads that had previously been within the gels is used to measure successful phagocytic engulfment. Both increased polymer concentration in agarose gels and increased cross-linking density in alginate gels are associated with a decreased success of phagocytic engulfment. Upon plotting the percentage of neutrophils showing successful engulfment as a function of the elastic modulus of the gel to which they were applied, it is found that data from both alginate and agarose gels collapse onto the same curve. This suggests that gel mechanics may be impacting the success of phagocytosis and demonstrates that this experiment is a step toward realizing methods for measuring how the mechanics of a large target, or a large structure in which smaller targets are embedded, impact the success of phagocytic engulfment.

SIGNIFICANCE Soft-tissue biofilm infections consist of multiple discrete ~100 μm aggregates of bacteria. ~10 μm neutrophils do not enter aggregates and are far too small to engulf them, although single bacteria are readily engulfed. By physical reasoning, for a cell attempting phagocytosis of a target, or target-containing structure, that is much larger than itself, success must depend on both the force exerted by the cell and on the mechanical properties of the large target or structure. This work is the first presentation of a way to measure how such mechanics affect phagocytosis. We show that the success of phagocytic engulfment may be impacted by elasticity for the range of moduli that we previously measured for biofilms regrown from clinical isolates.

INTRODUCTION

Neutrophils are short-lived phagocytic cells that are an integral part of the innate immune system and the most abundant white blood cell in humans (1–4). Phagocytosis is one of a neutrophil's main ways of clearing pathogens (5). Discrete, non-biofilm bacteria, each ~1 μm in size, are readily engulfed by neutrophils. However, biofilm infections in soft tissue are made up of many bacteria bound together in a polymeric matrix to form aggregates that cannot be cleared by neutrophils (6–8). Imaging studies of chronic biofilm infections show ~100-μm diameter aggregates that are densely surrounded by neutrophils that nevertheless do not enter the aggregates (9,10).

Neutrophils are ~10 μm in diameter and are unable to engulf rigid polystyrene particles (with Young's modulus ~3000 MPa) that are over ~10 μm in diameter (11). Size and other geometric characteristics like shape

Submitted February 6, 2019, and accepted for publication August 26, 2019.

*Correspondence: gordon@chaos.utexas.edu

Megan Davis-Fields and Layla A. Bakhtiari contributed equally to this work.

Editor: Cynthia Reinhart-King.

https://doi.org/10.1016/j.bpj.2019.08.043

also influence phagocytosis by macrophages, another type of phagocytic immune cell (12–15). A rigid bead 100 μm in diameter would be far too big to be phagocytosed by neutrophils (9–11,16). However, biofilms are not rigid solids but rather are composite viscoelastic materials. Such materials are often characterized by measuring their response to oscillatory shear. The elastic modulus G′ measures the energy-storing, solid-like response of the material, whereas the viscous modulus G″ represents the energy-dissipating, liquid-like response. We have shown that biofilms regrown from strains of *Pseudomonas aeruginosa* that were isolated from the lungs of cystic fibrosis (CF) patients at different points in time typically have elastic moduli in the range ∼1–10 kPa and loss moduli in the range ∼0.1–1 kPa (17). For most of these, G′ was at least an order of magnitude bigger than G″, indicating that these biofilms are dominantly solid like. Both of these findings are consistent with prior work by others measuring different types of *P. aeruginosa* biofilms (18–20). Furthermore, we found that in vivo evolution in chronic CF infections changed the production of matrix polymers in a way that promoted mechanical toughness (17).

An earlier study that combined numerical modeling with micropipette-based experiments found that neutrophils can exert a stress of ∼1 kPa while phagocytosing a small, rigid target (11); macrophages and blood granulocytes also exert stresses of ∼1 kPa during phagocytosis (12,21–23). Thus, the mechanical stress exerted by phagocytosing neutrophils (and other immune cells) is near the midpoint of the range of stiffnesses, or elastic moduli, of biofilms regrown from CF clinical isolates. Therefore, it is possible that variation in biofilm stiffness could impact biofilms' resistance to clearance by neutrophils and that the mechanical robustness promoted by evolutionary changes in polymer production could increase the infection's ability to evade phagocytic clearance by neutrophils. We expect that any phagocytosis of biofilm bacteria must take the form of small pieces of the biofilm being detached for subsequent engulfment. Indirect support for this idea comes from a recent finding that neutrophils can detach and engulf fragments of *Trichomonas vaginalis*, which is a pathogen too large for neutrophils to engulf whole (24–27). Neutrophils can also kill cancer cells using a similar "nibbling" process (28). These examples show that neutrophils have the ability to remove small pieces from a large target before engulfing those pieces. Phagocytosing *Dictyostelium* and *Entamoeba* can also break off and ingest small pieces of a target (29,30).

We expect that how successful neutrophils are at detaching pieces of biofilm or individual constituent bacteria for subsequent engulfment must depend on the mechanics of the biofilm material. Prior studies examining physical limitations of phagocytosis have focused on the size and shape of rigid targets, which are not good mechanical representations of biofilms (11–15). One earlier study using macrophages from mice showed that the stiffness of target particles could act as a cue for phagocytosis, with stiffer particles being more likely to be engulfed—however, the particles used were 6 μm or less in diameter and therefore well below the limiting size for phagocytosis (31). There have not been protocols for determining how mechanics impact the success of phagocytic engulfment when either the target itself is much bigger than the cell attempting phagocytosis or the target is embedded in a material much larger than the phagocytic cell. This hinders both fundamental understanding of neutrophil phagocytosis and the development of new types of treatments that could weaken biofilms to make them more susceptible to clearance by the immune system.

To be able to elucidate the mechanical limitations on phagocytic engulfment, we developed a method to determine the impact of mechanical properties on neutrophils' ability to engulf micron-sized beads that were initially embedded in centimeter-sized gels. Biofilms can produce chemical factors that kill neutrophils (32,33). This is an important component of biofilms' evasion of the immune system that we think is likely to interplay with biofilm mechanics. However, in this early stage of research, active killing of neutrophils by biofilm bacteria would be a confounding factor that could obscure the effects of mechanics per se. Therefore, to isolate the effects of mechanics, we use abiotic gels to recreate specific aspects of biofilm mechanics. Although in this initial development, we focus on solid-like stiffness, the gels we use are, like biofilms, viscoelastic; therefore, we anticipate that this method will be extensible to future study of how viscoelastic properties impact the success of, and the timescale for, phagocytic engulfment.

For two different hydrogel chemistries, alginate and agarose, we find that increasing either polymer concentration or cross-linking density is associated with lower success of phagocytic engulfment. We tentatively attribute this to a change in gel mechanics. As the elastic modulus of the gel varies across the range we previously measured for biofilms, the success of engulfment changes from ∼30% success at low stiffness to essentially 0% success at high stiffness. This is the first hint of a mechanical limit on phagocytosis. Thus, we demonstrate that a mechanical property is correlated with the degree of successful engulfment and that this experimental design is appropriate for probing the effects of stiffness, or elasticity, on phagocytosis by neutrophils. Therefore, this work constitutes a methodological development that can be used to advance the field and may constitute a step forward in basic understanding, pending further studies with additional gels.

METHODS

Microscopy

Laser-scanning confocal microscopy was done with an Olympus IX71 inverted confocal microscope, a 60× oil-immersion Olympus objective,

and FluoView FV10-AWS Ver 04.02. Except when stated otherwise, epifluorescence and phase contrast imaging was done using an inverted phase contrast microscope with 60× objective (both from Olympus), QImaging Exi Blue CCD camera, and QCapture Pro 6 software. For microscopy of alginate gels on coverslip chambers (product D35-14-1-U; Matsunami, Bellingham, WA), the coverslip was pretreated with 100 μL of 0.1% Poly-L-lysine (catalog number P9155; Sigma-Aldrich, St. Louis, MO) for 30 min to facilitate adhesion of the gel to the glass surface. The alginate gels made with 10 mM calcium consistently detached from the coverslip during imaging and therefore were not used for these experiments.

Hydrogel preparation

Alginate gels were made by dissolving 4% sodium alginate (catalog number 180947; Sigma-Aldrich) in distilled water and then adding a solution of 5% calcium carbonate ($CaCO_3$, catalog number C4830; Sigma-Aldrich) and 5% D-(+)-gluconic acid δ-lactone (GDL (catalog number G4750; Sigma-Aldrich). Final concentrations of 10, 20, and 30 mM $CaCO_3$ were used. 5% GDL was added to cause internal gelation by slowly lowering the pH of the gel, causing calcium ions to be released from $CaCO_3$ into solution (34).

We used pH paper (product P1119-1C; Cardinal Health, Dublin, OH) to measure pH before and after the addition of $CaCO_3$ and GDL (Fig. S1). The initial alginic acid solution had a pH of 8. For 10 mM calcium, the pH reduced to 6 or 7; for 20 or 30 mM calcium, the pH reduced to 6. Two replicates of each measurement were done.

Agarose gels were made using low-gelling temperature agarose (catalog number A9414; Sigma-Aldrich) at 0.3, 0.5, 1, 1.5, and 2%.

The synthesis of PEG diacrylate (PEGDA) was adapted from a published protocol (35). All materials for this synthesis were purchased from Sigma-Aldrich, unless stated otherwise. In brief, acryloyl chloride was added dropwise to the mixture solution of poly(ethylene glycol) (PEG) diol (35 kDa) in dichloromethane with triethylamine. The molar ratio of PEG diol, acryloyl chloride, and triethylamine was 1:2:4. After 24 h of reaction, 8 M excess of 2 M potassium carbonate solution was added to neutralize the unreacted acryloyl chloride. The reaction product was then precipitated with cold ether after the removal of residual water with sodium sulfate. After drying under ambient conditions for 24 h, the final PEGDA product was dried under vacuum for an additional 24 h.

PEGDA hydrogel slabs were fabricated by dissolving the PEGDA in deionized (DI) water at 4 and 10% polymer concentration. The UV initiator, Irgacure 2959 (1:100 weight ratio to the polymer), was added, and precursor solutions were then injected between 0.75-mm glass spacers and exposed to ultraviolet (UV) light (Intelli Ray Shuttered UV Flood Light, Integrated Dispensing Solutions, 365 nm, 4 mW/cm^2) for 6 min per side to initiate radical cross-linking.

When used for engulfment assays, all three gels contained 10 mg/mL bovine serum albumin (BSA) (HycClone brand, catalog number SH30574.01; purchased from GE Life Sciences, Chicago, IL).

Alginate and agarose gels used for engulfment assays contained fluorescent beads (polystyrene Dragon Green beads, diameters 0.955 μm, catalog number FSDG004; Bangs Laboratories, Fishers, IN), which were diluted volumetrically by a factor of 100 when they were added to the solution before gelling. According to data supplied by Bangs Laboratories, the original suspension of beads contained $\sim 1.8 \times 10^{11}$ beads per milliliter, so the dilution results in $\sim 1.8 \times 10^{9}$ beads per milliliter of gel. Each bead has a volume of less than 10^{-12} mL. Thus, the volume fraction of beads in the gel is $\sim 10^{-3}$. Although the inclusion of rigid beads or powders by soft materials can result in changes in material properties, such as an abrupt increase in brittleness or stiffness, the volume fraction of embedded particles required to achieve the associated percolation transition is between 0.4 and 0.6 (36,37).

PEGDA gels used for engulfment assays did not contain beads but were prepared with a modified protocol so that gels would be fluorescent. PEGDA precursor solutions in HBSS were prepared as described above with the addition of 0.01 mg/mL BSA and 200 μg/mL FITC-o-acrylate, both purchased from Sigma-Aldrich. The acrylate group on the FITC reacts with the end of the PEG chain and thus becomes conjugated to the gel. Hydrogel slabs were swollen in 200 μL HBSS overnight and then rinsed with HBSS three times to remove unconjugated FITC-o-acrylate before incubating with neutrophils.

Hydrogels used for microscopy experiments were stored overnight at 4°C in 500-μL aliquots in 24-well flat-bottom plates (catalog number 15705-060; Corning, Corning, NY). Alginate and agarose hydrogels used for rheological measurements were poured into petri dishes (60-mm diameter) at 1000–2000 μm deep and stored overnight at 4°C.

Rheology

Oscillatory bulk rheology was done using a stress-controlled AR 2000ex rheometer (TA Instruments, New Castle, DE). Hydrogel samples were taken out of 4°C storage on the morning of the experiment and placed at 37°C for 1 h. Then, alginate and agarose gel sections were placed on the rheometer and cut down to the size of the 8-mm parallel plate head. PEGDA gels for rheological measurements were swollen in DI water overnight before specimens were punched from the slab with an 8-mm biopsy punch.

The height of the tool gap varied between 1 and 2 mm; this was used to determine the depth of the gels. Oscillatory frequency sweeps from 0.1 to 600 rad/s at 1% strain, and strain sweeps from 0.1 to 200% at 3.14 rad/s were performed on each sample on each day of measurement. Elastic modulus was taken as the midpoint of the G′ plateau region for strain sweeps. Three replicate rheology measurements were done on bead-free gels for each concentration of agarose, calcium, and PEGDA used. In addition, two more replicate rheology measurements were done for each type of bead-containing agarose and alginate gels at the bead concentration used for engulfment measurements.

Bracketing gel pore size

100 μL solutions of alginate (made with 20 and 30 mM calcium) and 0.3% agarose were deposited on and allowed to gel on coverslip-bottomed dishes. The gel covered half of the coverslip so that the leading edge could be easily visualized. Solutions containing either a 1:100 dilution of 200 nm fluorescent polystyrene beads (catalog number FSDG002; Bangs Laboratories) or 2000 K molecular weight dextran (catalog number D7137; Thermo Fisher Scientific, Waltham, MA) were then deposited next to the gel; dextran of this size has a hydrodynamic radius of 35 nm (38). Confocal z-stack micrographs were acquired.

Neutrophil isolation

Neutrophil work was approved by the Institutional Review Board at the University of Texas at Austin (Austin, TX) as Protocol Number 2015-05-0036.

Human neutrophils were isolated from two adult volunteer blood donors following a published protocol (39). In brief, blood was collected in lithium heparin-coated tubes (BD Vacutainer, catalog number 367880), mixed with a filter-sterilized (catalog number 28145-501; filters from VWR, Radnor, PA) 3% dextran and 0.9% sodium solution (catalog numbers 31392 and S9888; Sigma-Aldrich). Red blood cells fell out of solution. The resulting supernatant was centrifuged (Eppendorf 5810R, A-4-62 Rotor, with swinging buckets with 15 mL conical tube adapters) for 10 min at 500 × g, and the resulting pellet was resuspended in 10 mL of Hanks Buffered Salt Solution (HBSS) (catalog number 14175095; Gibco Laboratories, Gaithersburg, MD) without calcium or magnesium. Cells were separated using a Ficoll-Paque density gradient solution (catalog number 17-1440-02; GE Healthcare, Chicago, IL), spun at 400 × g for 40 min. This resulting pellet was resuspended in DI water for 30 s to lyse any remaining red blood cells.

Then, the isotonicity of the solution was restored using a filter-sterilized 1.8% NaCl solution (catalog number S9888; Sigma-Aldrich). Cells were centrifuged for 5 min at 500 × *g*, and the final neutrophil pellet was resuspended in 1 mL HBSS with calcium and magnesium (catalog number 14025092; Gibco Laboratories) and 20% human serum (catalog number H4522; Sigma-Aldrich). This medium was used for all neutrophil experiments.

Neutrophil engulfment assay and microscopy for agarose and alginate gels

On the day of phagocytic engulfment experiments, neutrophils were isolated as described above. While neutrophils were being isolated, 100 μL of rabbit anti-BSA antibody (catalog number A11133; Invitrogen, Carlsbad, CA) diluted 1:1000 in Dulbecco's phosphate-buffered solution (catalog number 14190144; Gibco Laboratories) was added to each hydrogel and incubated at 4°C for 30 min. Hydrogels were then washed three times with Dulbecco's phosphate-buffered solution, and 200 μL of freshly isolated neutrophil suspension was added to each well. The hydrogel plate with neutrophils was then incubated at 37°C for 1 h; 37°C is human body temperature. After 1 h, the solution containing cells was collected from off the top of the hydrogel. In some cases, to increase the number density of cells in the microscope field of view, collected neutrophils were concentrated and resuspended in 50 μL of HBSS. The collected cells were put on a microscope slide with a coverslip and Grace labs imaging spacer (catalog numbers 12-550-15 and 12-541-B, Thermo Fisher Scientific; and catalog number GBL654004, Sigma-Aldrich). Before using with cells, coverslips had been coated in 0.1% poly-L-lysine (catalog number P9155; Sigma-Aldrich) for 30 min and then triple rinsed. Cells were imaged using phase contrast microscopy, and beads were imaged using epifluorescence microscopy with a filter for green fluorescent protein. At least 100 neutrophils from every sample, from fields of view chosen at random, were counted as either containing or not containing fluorescent beads, which served as indicators of gel engulfment. Replicate numbers were as follows: 5 for 0.3% agarose and 4 for all other agarose concentrations and for all alginate gels.

Engulfment assay with PEGDA gels

8-mm punches of PEGDA gel were placed in a 24-well plate, and each swelled overnight with 200 μL of HBSS buffer. 100 μL of anti-BSA antibodies at 1:1000 dilution were applied to the gels for 30 min, after which each gel was rinsed three times with HBSS buffer medium. 200 μL of freshly isolated neutrophil suspension was added to each gel and incubated for 1 h. Cells were then collected from the gel substrate, concentrated, and counted from confocal micrographs. Three replicate experiments were done for each PEGDA gel concentration used.

Growth of bacterial aggregates

Overnight shaken cultures of *P. aeruginosa* naturally contain both multicellular aggregates and single cells (40). To promote the formation of more and larger aggregates, we used a lab strain of bacteria that overexpresses the extracellular polysaccharide Psl, *ΔwspF Δpel* (41). The background for this lab strain is the University of Washington version of PAO1 (42,43). A ΔwspF Δpel mutant of PAO1 previously developed by other researchers (44) was later modified to express green fluorescent protein (41) and subsequently used in this work.

We grew aggregates using the same process we have described previously (45,46). Frozen bacterial stock was streaked onto a lysogeny broth agar petri plate and incubated at 37°C overnight. From this plate, one colony was dispersed into 4 mL of lysogeny broth liquid growth medium and left to overgrow for ~20 h at 37°C on a rotating shaker (Labnet Orbit 1000, 242 rotations per minute), inside a Thermo Fisher Scientific Isotemp Incubator. Overgrowth to stationary phase increased the number of large multicellular aggregates present.

Microscopy of neutrophils and bacterial aggregates

Freshly isolated human neutrophils at a concentration of $\sim 10^6$ cells/mL were mixed with bacterial culture (diluted to $OD_{600} = 0.2$ measured using a Spectronic 20 Genesys spectrophotometer) and placed on a coverslip chamber for imaging using time-lapse phase contrast microscopy. As described in our previous work, the stage region of this microscope is enclosed in an incubator chamber, custom-built by Precision Plastics (Columbia City, IN) (41,47,48). During image acquisition, the microscope stage incubator was set to 37°C, human body temperature. Images were analyzed using Fiji, a software distribution of ImageJ. A total of 810 (Video S1), 199 (Video S2), and 4500 (Video S3) frames were acquired for each video.

Microscopy videos of neutrophils excluded by gels

100 μL solutions of alginate (with 20 mM or 30 mM calcium) and of 0.3 and 1% agarose were deposited on and allowed to gel on coverslip-bottomed dishes. Agarose gels made with 0.3 and 0.5% agarose were used because they were the softest agarose gels used in our engulfment assays, for which we measured the greatest success of phagocytic engulfment. The gel covered half of the coverslip surface so that the boundary with solution could be easily visualized. Time-lapse phase contrast micrograph videos were then acquired at the gel boundary to visualize whether neutrophils were able to penetrate each gel. Videos of neutrophils on alginate gels were acquired with a Hamamatsu Orca-Flash 4.0 (C11440) camera and MetaMorph Advanced Version 7.7.6.0.

Height profile of neutrophils excluded by gel

A solution of 0.3% agarose containing BSA and 1-μm fluorescent beads was gelled on top of the coverslip portion of a coverslip dish. The dish was stored at 4°C for ~1 h before use. A water-soaked paper towel piece was left inside the dish, and the lid was tightly sealed with parafilm to prevent the gel from drying out before use. 100 μL of freshly isolated neutrophil suspension were deposited on the top surface of the gel, and confocal microscopy *z*-stacks imaging both gel and neutrophils were collected for 2 h. The fluorescence images for each time point were analyzed using the Fiji distribution of ImageJ. A threshold was applied to better visualize beads, and the built-in ImageJ Analyze Particles function was used to filter out-of-focus particles from each frame. The reported bead count from this function was then plotted in Excel as a function of slice and, thus, height. The number of neutrophils in focus at the midsection of each cell per frame was counted manually and recorded as a function of *z*-slice and, thus, height.

Statistics

Statistical analysis was done using Microsoft Excel.

RESULTS

Measurements of neutrophil interactions with biofilms

To assess whether neutrophils could remove individual bacteria from biofilms and to estimate the timescale for such a process, time-lapse phase contrast microscopy was used to

image neutrophils interacting with biofilm-like bacterial aggregates that were an order of magnitude bigger than the neutrophils. On several occasions, we saw neutrophils remove and engulf one or two bacteria out of an aggregate (Figs. S2–S4; Videos S1, S2, S3, S4, and S5).

For many viscoelastic materials, including the gels used in this study, the elastic and viscous moduli measured depend on the frequency of oscillatory shear. Estimating the frequency characterizing the strain imposed by neutrophils will allow determination of what frequency regime is relevant for this study. For this, five protrusions of different sizes, from four different attacking neutrophils, were observed, and the time that elapsed during each retraction of a protrusive appendage was measured. The inverse of this time was taken to be the frequency characterizing the strain that could be imposed by the retraction of that particular protrusion. On average, this frequency was 0.06 Hz, with a standard error of the mean of 0.01 Hz; 0.06 Hz is approximately equivalent to an angular frequency of 0.38 radians/s. The average observed distance covered by protrusions at their maximal extension was 2.97 μm (standard error of the mean (SEM) 0.28 μm), and the estimated average speeds were 0.26 μm/s (SEM 0.13 μm/s) for extension and 0.18 μm/s (SEM 0.10 μm/s) for retraction. Others have measured the leading edge of a neutrophil protrusion wrapping around a bead at 0.1 μm/s, which is comparable to the speeds we measure (11).

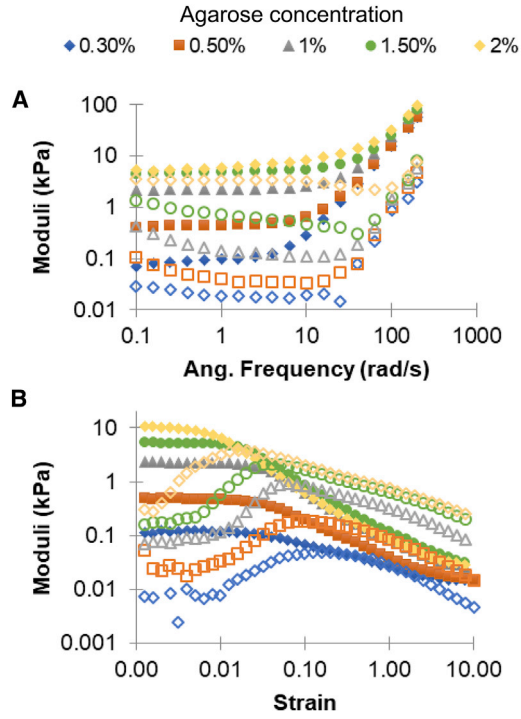

FIGURE 1 Representative (*A*) frequency and (*B*) strain sweeps, all from the same day of measurement, for agarose gels ranging in concentration from 0.3% agarose to 2% agarose. Frequency sweeps were done at 1% strain, and strain sweeps were done at 3.14 radians/s. The elastic moduli (G′) are shown with solid symbols, and the viscous moduli (G″) are shown with hollow symbols of corresponding shape and color. To see this figure in color, go online.

Mechanical properties of hydrogels

The mechanical properties of the hydrogels used in this study were measured using oscillatory bulk rheology. Before rheology, the gels were placed in a 37°C incubator for 1 h to ensure the mechanics being measured were the same as those in the engulfment experiments in which we exposed gels to neutrophils at 37°C (49). Two primary hydrogel types, agarose and alginate, were used so that the elastic moduli could be varied across comparable ranges using two different chemical compositions. Alginate is an important component of the biofilm matrix for many strains of *P. aeruginosa*.

Agarose gels

Agarose is a linear polymer with alternating D-galactose and 3,6-anhydro-L-galactose units. Increasing the concentration of polymer in a gel will increase the gel's elastic modulus (50). Using agarose concentrations from 0.3 to 2%, the resulting range of elastic moduli, ~0.1 to ~10 kPa (Fig. 1), roughly covered the range of elastic moduli that we measured previously for biofilms grown from clinical isolates of *P. aeruginosa* (17). Adding BSA and polystyrene beads to the gels, as for engulfment measurements, did not significantly impact the mechanics of the gels (Fig. S5 *A*; Table 1). The value of the elastic modulus at the midpoint of the plateau region in strain sweeps is the value used herein to characterize these gels' mechanics, unless the material was already yielding for the lowest strain used–in that case, the value of the elastic modulus that was measured at the lowest strain was used (Fig. 1 *B*). For each concentration of bead-free agarose, three replicates were made, and the measured elastic moduli were averaged (Table 1). For gels containing BSA and beads, two replicates each were made and measured (Table 1).

Alginate

Alginate polymers are made up of β-D-mannuronate and α-L-guluronate residues. Divalent calcium ions cross-link the α-L-guluronate residues of alginate polymers, and increasing this cross-linking density is known to increase the elastic moduli of alginate gels (51). This is consistent with what we found using bulk rheology (Fig. 2). Adding BSA and polystyrene beads did not impact the mechanics of the gels (Fig. S5 *B*; Table 2). Calcium concentrations of 10, 20, and 30 mM resulted in elastic moduli of the alginate gels ranging from 0.1 to 4.5 kPa. The elastic modulus used herein is the value at the midpoint of the plateau region of the strain sweep. For bead-free gels, for each concentration of calcium used, three replicate alginate gels were made, and the measured values averaged to determine the elastic modulus (Table 2). For gels containing BSA and beads,

TABLE 1 Moduli Measured for Gels Made of Different Concentrations of Agarose

Agarose concentration	0.30%	0.50%	1.0%	1.5%	2.0%
Agarose Gels ($n = 3$)					
Elastic Shear Modulus (SEM) in Pascals	125 (3)	370 (60)	2250 (70)	5600 (300)	10,500 (700)
Agarose Gels containing BSA and polystyrene beads ($n = 2$)					
Elastic Shear Modulus (SEM) in Pascals	120 (20)	320 (190)	1700 (370)	5200 (600)	8700 (1800)

two replicate gels were made and measured for each calcium concentration (Table 2).

At the low frequencies characterizing neutrophil-imposed deformations of in vitro biofilm aggregates, the elastic moduli have no significant dependence on frequency for all gels used (Figs. 1 *A* and 2 *A*).

Measurement of the success of phagocytic engulfment

As an indicator of the success of phagocytic engulfment, we used phase contrast and epifluorescence microscopy to determine the percentage of neutrophils that, after 1 h's incubation with a gel, contained fluorescent beads that had originally been embedded within the hydrogel. For each sample, at least 10 fields of view under the microscope were chosen at random, and at least 100 neutrophils were counted. Four or five replicate experiments were done, on different days, for each agarose or calcium concentration. The hydrogels were in the centimeter-sized bottoms of 24-well plates and much larger than the neutrophils themselves, so that the shape of the gel presented to neutrophils was a flat surface, approximating the surface of a spheroid much larger than a neutrophil.

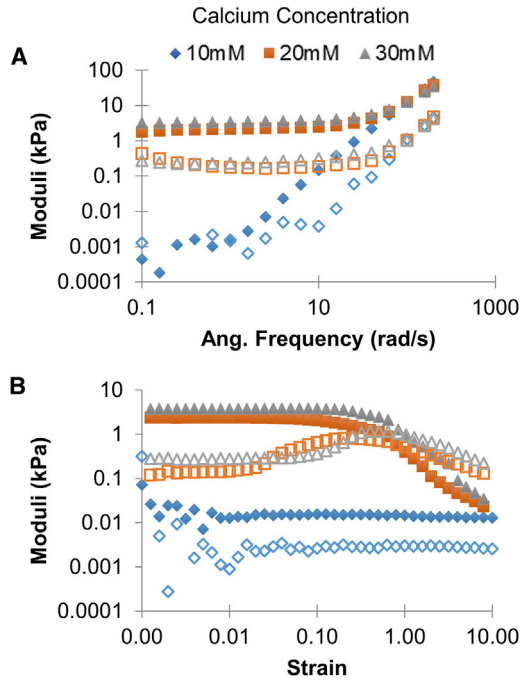

FIGURE 2 Representative (*A*) frequency and (*B*) strain sweeps, all from the same day of measurement, for alginate gels made with 10, 20, and 30 mM calcium. Frequency sweeps were done at 1% strain, and strain sweeps were done at 3.14 radians/s. The elastic moduli (G′) are shown with solid symbols, and the viscous moduli (G″) are shown with hollow symbols of corresponding shape and color. To see this figure in color, go online.

Alginate

For alginate gels cross-linked with 10, 20, and 30 mM calcium, on average, 77, 5, and fewer than 2%, respectively, of neutrophils internalized beads that had been initially embedded in a gel (Figs. 3 and 4).

Agarose

The fraction of neutrophils containing beads that had originally been contained in agarose gels decreases sharply upon changing agarose concentration from 0.3 to 0.5% (Fig. 5). For 0.3% agarose gels, on average, 28% of neutrophils had internalized fluorescent beads. For gels at 0.5% agarose and above, on average, less than 2% of neutrophils internalize fluorescent beads.

Gel mesh size and neutrophil exclusion

To assess the degree to which different amounts of successful engulfment arise from different gel mesh sizes, we use, as tracers, diffusible fluorescent molecules and beads, applied to the fluid medium outside gels. Alginate gels made with 20 and 30 mM calcium and 0.3% agarose gels all exclude 200 nm fluorescent beads (Videos S6, S7, S8, S9, S10, and S11). This indicates that pores are smaller than 200 nm for all three of these gels and that ~10 μm neutrophils are unlikely to migrate through gels. We find that

TABLE 2 Moduli Measured for Alginate Gels Made with Different Concentrations of Cross-Linking Calcium Ions

Calcium concentration	10 mM	20 mM	30 mM
Alginate Gels ($n = 3$)			
Elastic Shear Modulus (SEM) in Pascals	13 (1)	1500 (500)	4500 (300)
Alginate Gels with BSA and polystyrene beads ($n = 2$)			
Elastic Shear Modulus (SEM) in Pascals	60 (20)	1400 (440)	2800 (50)

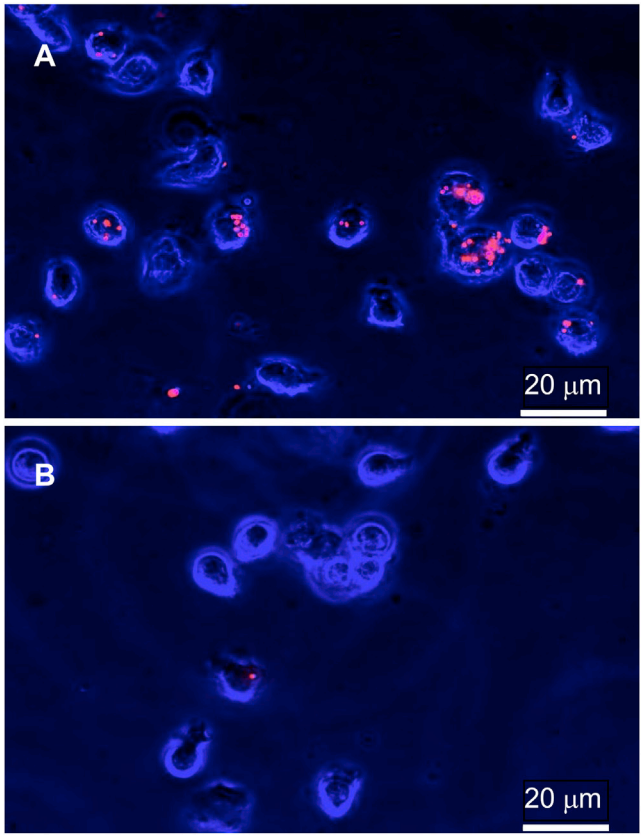

FIGURE 3 False-colored phase contrast images of neutrophils (*blue*) combined with fluorescence images of beads (*red*) after incubation with alginate gels cross-linked with 10 mM calcium (*A*) and 30 mM calcium (*B*). Neutrophil populations that were incubated with gels of lower elasticity (cross-linked by 10 mM calcium) have a larger proportion of neutrophils with internalized beads than those populations that were incubated with gels of higher elasticity (cross-linked by 30 mM calcium). To see this figure in color, go online.

35 nm dextran enters the 0.3% agarose gel readily but not alginate gels made with 20 and 30 mM calcium (Videos S12, S13, S14, S15, and S16). This indicates that the lowest-concentration agarose gel we use has larger pores

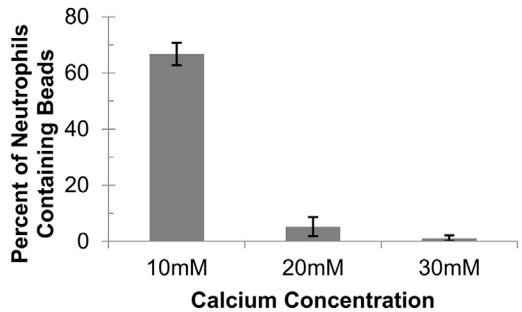

FIGURE 4 Neutrophils more successfully engulf beads when the embedding alginate gels are cross-linked with lower concentrations of calcium. As the concentration of calcium increases and therefore calcium cross-linking increases, the ability of neutrophils to successfully engulf beads decreases. Error bars are standard error of the mean. Single-factor analysis of variance gives a p-value of 5×10^{-8}.

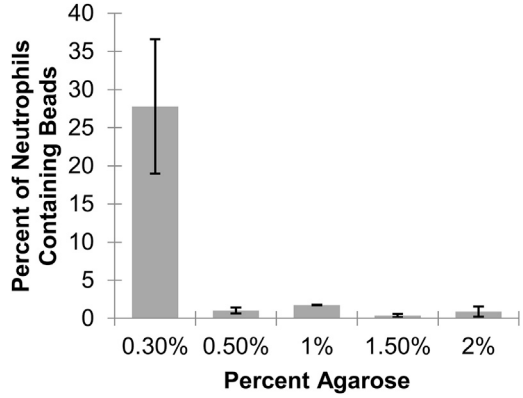

FIGURE 5 Neutrophils more successfully engulf beads when the embedding agarose gels are made with low concentrations of agarose. At 0.3% agarose, an average of 28% of neutrophils had internalized beads. For all other agarose concentrations, fewer than 2% of neutrophils had internalized beads. Error bars are standard error of the mean. Single-factor analysis of variance gives a p-value of 0.002.

than the two more cross-linked alginate gels. The pore sizes we bracket using diffusible tracers are reasonably consistent with pore sizes reported for similar alginate and agarose gels (52–57).

To directly assess whether neutrophils or their visible ($\sim$1 μm) protrusions enter gels, we took time-lapse microscopy videos of neutrophils crawling along one edge of bead-containing agarose and alginate gels (Videos S17, S18, S19, S20, S21, and S22). In no case was a neutrophil or protrusion seen to enter a gel.

Finally, for the 0.3% agarose gel, for which we measured the greatest successful engulfment, we applied neutrophils to the top of a gel and imaged them under the confocal microscope over 2 h, which is twice the duration of our engulfment experiment (Videos S23, S24, and S25). We identified the volume of the gel using embedded beads and the top of the gel as the z-position where the bead density abruptly began to drop. Over 2 h, the neutrophils were consistently localized at the top of the gel (Fig. 6).

Therefore, we conclude that neutrophils do not migrate through the alginate and agarose gels we use for engulfment experiments. This parallels findings that neutrophils do not enter biofilms in vivo (9,10). The pore sizes we bracket for alginate and agarose gels are also consistent with previous measurements of biofilm pore sizes (38).

Successful engulfment correlates negatively with the elastic modulus of the gel

For this biofilm-mimicking regime, using both alginate and agarose gels allows a preliminary disentangling of the effects of stiffness from any effects arising from specific chemical composition. For both hydrogels, the percentage of neutrophils that successfully engulfed beads varies with

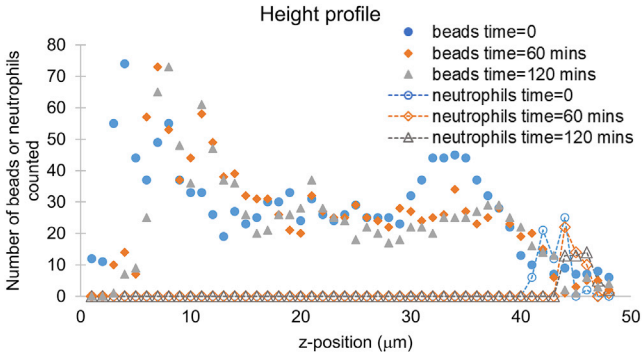

FIGURE 6 Neutrophils were applied to the top of a bead-containing 0.3% agarose gel. The gel plus neutrophils were imaged on the confocal microscope immediately after neutrophils were added, 1 h later, and 2 h later. The number of beads visible in each frame (solid symbols) were counted to determine where the gel top was located because the liquid medium was free of beads. Neutrophils (*hollow symbols*) were counted for the frames where their midplanes were in focus. Dashed lines connecting neutrophil counts are a guide to the eye. To see this figure in color, go online.

the stiffness in such a way that data from the two types of gel lie very nearly along the same curve (Fig. 7).

Engulfment of bead-free gel

To probe whether phagocytosis would happen in the absence of beads and thereby assess whether the gel itself can be a target for phagocytosis as opposed to the beads per se being targets embedded in a larger, nontarget structure, we require a gel that can be labeled for visibility under the microscope. For this, we use PEGDA gels that were labeled by covalently bound fluorescein isothiocyanate (FITC), and neutrophils that have engulfed part of such gels are identifiable by confocal fluorescence microscopy (Fig. 8). PEGDA gels containing 4 and 10% 35 kDa PEGDA have elastic moduli of ~200 and ~2000 kPa. On average, 7% of neutrophils exposed to PEGDA gels contained internal FITC (SEM 1.2%). This is roughly twice the percentage of neutrophils

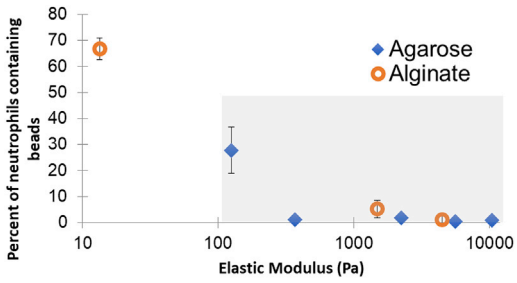

FIGURE 7 The percentage of neutrophils that have engulfed beads decreases as the elastic modulus of agarose or alginate hydrogel increases. Elastic moduli are from measurements of gels without beads. Error bars are standard error of the mean. The gray shaded region indicates the range of elastic moduli that we measured earlier for biofilms regrown from clinical isolates taken from patients with cystic fibrosis. To see this figure in color, go online.

that were determined to have achieved successful engulfment, using tracer beads, for agarose and alginate gels with about the same range of elastic moduli.

DISCUSSION

Interpreting measurements of successful engulfment

Alginate and agarose gels are advantageous for this study because they are chemically similar to the extracellular polysaccharides that scaffold biofilm matrices; indeed, alginate is an important component of many *P. aeruginosa* biofilms (58–60). However, alginate and agarose gels are not readily distinguishable from aqueous culture medium under the microscope and therefore we use embedded beads as tracers to allow us to determine whether engulfment has occurred. The use of tracer beads means that at least two interpretations of our engulfment measurements (Figs. 4 and 5) are possible. In one view, the gel itself is the target for phagocytosis, and beads are engulfed when, by happenstance, they are contained in the piece of gel that is detached. In another view, the beads themselves are the target for phagocytosis. Neutrophils might sense rigid beads that contrast mechanically with the surrounding, soft gel and pluck out beads on or near the gel surface. The latter interpretation is indirectly supported by work showing that the stiffness of target particles can act as a cue for phagocytosis by macrophages, with stiffer particles being more likely to be engulfed (31). In our case, this might involve infiltration of suboptical filipodia (~0.2 μm in width) into the top of the gel, along the surface of an embedded bead and subsequent formation of a phagocytic cup over the bead, leading to engulfment; steps of such a process have been shown using electron microscopy (61,62).

There are at least three possible reasons that FITC-labeled PEGDA gels may give rise to higher measurements of successful engulfment than do bead-containing alginate and agarose gels. First, to avoid perturbing gel mechanics, we use only a low concentration of beads. This leaves regions of bead-free gel with sizes comparable to or larger than neutrophils; in contrast, the labeled PEGDA gels contain FITC throughout. Therefore, pieces of agarose and alginate gel may be engulfed without tracer beads; if so, the actual rate of successful engulfment is being undercounted in those experiments. Second, when PEGDA gels are formed containing beads, as for the agarose and alginate gels, the beads rapidly diffuse out of the PEGDA gel (for this reason, PEGDA gels containing beads were not used for engulfment measurements). This indicates that the pore sizes for the PEGDA gels used are comparable to or greater than the 1-μm bead diameter compared with pore sizes less than 200 nm for alginate and agarose gels. It is plausible that larger pores might impact the interaction of neutrophils with gels. Finally, we cannot discount the possibility that

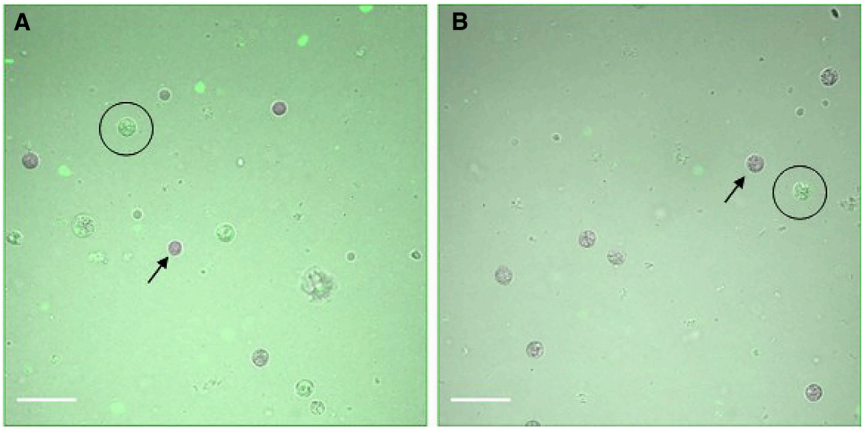

FIGURE 8 Confocal z-slices of neutrophils that had been exposed to FITC-labeled (*A*) 4% and (*B*) 10% PEGDA gels for 1 h. In each frame, a FITC-containing neutrophil is circled, and a neutrophil that does not contain FITC is indicated with an arrow. Scale bars represent 30 μm. To see this figure in color, go online.

gel chemistry may be playing a role in immunogenicity or in adhesion to the surface and/or subsequent phagocytic engulfment.

Thus, the FITC-dyed PEGDA gels have significant structural and chemical differences from the bead-containing alginate and agarose gels. Therefore, although our results on PEGDA gels suggest that the gel itself can be a target for phagocytosis, this does not exclude the possibility that, in bead-containing agarose and alginate gels, it is actually the rigid embedded beads that are the only or primary targets for phagocytosis. Both of these possibilities are consistent with gel mechanics impacting the success of engulfment.

Correspondence with biofilms

P. aeruginosa cells have a Young's modulus in the low tens of MPa and, thus, are at least three orders of magnitude stiffer than the biofilm in which they are embedded (63). The tracer beads we use are made of polystyrene, which has a Young's modulus in the low thousands of MPa and, thus, are at least five orders of magnitude stiffer than the agarose or alginate gel in which they are embedded. Thus, there is a somewhat similar mechanical contrast between beads and embedding gel and biofilm bacteria and embedding matrix.

Notably, both the chemical composition and the mesh sizes of alginate and agarose gels are much closer to what is found in biofilm matrices than are the chemical composition and mesh sizes of PEGDA gels.

Other potential influences on neutrophil engulfment

The studies in this article focus on the elastic modulus of large, gel targets. However, the yield strain and stress, toughness, and compliance as well as other mechanical properties could influence the success of phagocytosis as well. Failure strengths of several thousand up to nearly 20,000 Pa have been measured for biofilms but at strain rates much greater than those applied by neutrophils; this suggests that new measurements of biofilm failure, at low strain rates, are needed (64,65). Furthermore, the strength of the adhesion of the phagocytic cell to the target could also impact the success of phagocytosis.

To engulf particles, neutrophils must bind to the target as it extends its cell membrane to engulf the target. The more binding sites, the stronger a neutrophil can adhere and wrap itself around the target (11,66). Here, to make the abiotic gels recognizable to the neutrophils, BSA was added into the gel and was then incubated with an anti-BSA antibody before exposure to the neutrophils. Previous studies of the mechanical limitations of neutrophil phagocytosis have been measured only with antibody-mediated phagocytosis (11,66). This method has been used to study neutrophil mechanics when the target is a stiff, polystyrene bead (11,66). In the studies presented here, the presence or absence of antibodies did not affect the success of engulfment when neutrophils were applied to bead-containing alginate gels. BSA was still added to the gels, but as engulfment occurs without the antibodies present, this phagocytosis may not be mediated through the Fc receptors.

Work on macrophages, another type of phagocytic immune cell, indicates that the stiffness of the culturing substrate or of the target itself may impact phagocytosis by promoting phagocytosis or related phenotypic changes through macrophage mechanobiology (67–70). How such effects may interplay with the mechanical limitation we study here are not known.

Implications for biofilm disease

The range of elastic moduli recreated by agarose and alginate gels includes the range of elastic moduli that we previously measured for biofilms grown from clinical bacterial isolates, ~0.05–10 kPa (17). This range is indicated by the gray box in Fig. 7. For gels with moduli spanning this range, the measured success of neutrophils at detaching and engulfing parts of the gel falls from ~30% success to ~0% success. This suggests that the elastic modulus of biofilm infections might impact their resistance to the immune system and

that the evolutionary trend toward promoting biofilm toughness that we showed in our earlier work (17) may reflect a selective advantage of higher elasticity for biofilms.

The increased resistance to phagocytosis conferred by increased elastic modulus of biofilms could result in worse outcomes for infected patients if it causes frustrated phagocytosis, in which neutrophils release reactive oxygen species that damage host tissue as well as bacteria (71,72). Indeed, damage from the patient's own inflammatory response and an associated release of reactive oxygen species is the primary cause of lung failure in CF patients (73,74). Mechanical resistance to phagocytosis could also allow more time for bacterial virulence factors, such as pyocyanin and rhamnolipids produced by *Pseudomonas aeruginosa*, to be produced and to damage neutrophils (32,33).

CONCLUSION

We have made significant progress toward developing a method for determining how the mechanics of a large target, or a large structure in which targets are embedded, impact the phagocytic success of an attacking cell. Future work could extend this method to other gel chemistries to examine the effect of other mechanical properties of the target, such as yielding, and of the mechanical forces binding the phagocytic cell to the target. The use of gels with specifically tunable yield strains and surface chemistries, as well as elastic moduli, would be desirable for this. Our study here measures phagocytic success only after a fixed time, but our method is readily extensible to time-varying studies to determine how mechanics impacts the timescale for successful engulfment; we speculate that truly viscoelastic properties, such as compliance, may strongly impact this timescale.

As we and others continue to develop the method presented here and extend these studies as outlined in the preceding paragraph, we expect to be able to determine what mechanical properties render a biofilm most susceptible to phagocytic clearance. We expect that this will guide us and other researchers as we work to develop new, nonantibiotic approaches to biofilm treatment, which we hope will circumvent biofilm's innate, phenotypic resistance to antibiotics, reduce damage to patients' health by the harmful side effects of antibiotics, and slow the evolutionary development of antibiotic resistance.

SUPPORTING MATERIAL

Supporting Material can be found online at https://doi.org/10.1016/j.bpj.2019.08.043.

AUTHOR CONTRIBUTIONS

M.D.-F. and L.A.B. performed experiments, analyzed data, and wrote the article. M.D.-F. and L.A.B. contributed equally to this article. Z.L., L.W., and K.N.K. performed experiments. E.M.C.-H. designed research. V.D.G. designed research and wrote the article.

ACKNOWLEDGMENTS

We thank Prof. Nathaniel A. Lynd (Department of Chemical Engineering, The University of Texas at Austin) for the use of his rheometer and for helpful discussions. We thank Prof. Laura Suggs (Department of Biomedical Engineering, The University of Texas at Austin) for helpful discussions and assistance with the alginate gel. Neutrophil work was approved by the Institutional Review Board at the University of Texas at Austin as Protocol Number 2015-05-0036.

This work was supported by grants from the Cystic Fibrosis Foundation (Gordon1710), the National Institutes of Health (1R01AI121500-01A1, National Institute of Allergy and Infectious Diseases), and the National Science Foundation (727544; Biomechanics and Mechanobiology; Civil, Mechanical, and Manufacturing Innovation), all to V.D.G.

REFERENCES

1. Amulic, B., C. Cazalet, …, A. Zychlinsky. 2012. Neutrophil function: from mechanisms to disease. *Annu. Rev. Immunol.* 30:459–489.
2. de Oliveira, S., E. E. Rosowski, and A. Huttenlocher. 2016. Neutrophil migration in infection and wound repair: going forward in reverse. *Nat. Rev. Immunol.* 16:378–391.
3. Kubes, P. 2018. The enigmatic neutrophil: what we do not know. *Cell Tissue Res.* 371:399–406.
4. Craig, A., J. Mai, …, S. Jeyaseelan. 2009. Neutrophil recruitment to the lungs during bacterial pneumonia. *Infect. Immun.* 77:568–575.
5. Lovewell, R. R., Y. R. Patankar, and B. Berwin. 2014. Mechanisms of phagocytosis and host clearance of *Pseudomonas aeruginosa*. *Am. J. Physiol. Lung Cell. Mol. Physiol.* 306:L591–L603.
6. Jesaitis, A. J., M. J. Franklin, …, Z. Lewandowski. 2003. Compromised host defense on *Pseudomonas aeruginosa* biofilms: characterization of neutrophil and biofilm interactions. *J. Immunol.* 171:4329–4339.
7. Kobayashi, S. D., N. Malachowa, and F. R. DeLeo. 2018. Neutrophils and bacterial immune evasion. *J. Innate Immun.* 10:432–441.
8. Hirschfeld, J. 2014. Dynamic interactions of neutrophils and biofilms. *J. Oral Microbiol.* 6:26102.
9. Kirketerp-Møller, K., P. Ø. Jensen, …, T. Bjarnsholt. 2008. Distribution, organization, and ecology of bacteria in chronic wounds. *J. Clin. Microbiol.* 46:2717–2722.
10. Kragh, K. N., M. Alhede, …, T. Bjarnsholt. 2014. Polymorphonuclear leukocytes restrict growth of *Pseudomonas aeruginosa* in the lungs of cystic fibrosis patients. *Infect. Immun.* 82:4477–4486.
11. Herant, M., V. Heinrich, and M. Dembo. 2006. Mechanics of neutrophil phagocytosis: experiments and quantitative models. *J. Cell Sci.* 119:1903–1913.
12. Champion, J. A., A. Walker, and S. Mitragotri. 2008. Role of particle size in phagocytosis of polymeric microspheres. *Pharm. Res.* 25:1815–1821.
13. Champion, J. A., and S. Mitragotri. 2006. Role of target geometry in phagocytosis. *Proc. Natl. Acad. Sci. USA.* 103:4930–4934.
14. Doshi, N., and S. Mitragotri. 2010. Macrophages recognize size and shape of their targets. *PLoS One.* 5:e10051.
15. Paul, D., S. Achouri, …, P. Cicuta. 2013. Phagocytosis dynamics depends on target shape. *Biophys. J.* 105:1143–1150.
16. Bjarnsholt, T., M. Alhede, …, N. Høiby. 2013. The in vivo biofilm. *Trends Microbiol.* 21:466–474.
17. Kovach, K., M. Davis-Fields, …, V. Gordon. 2017. Evolutionary adaptations of biofilms infecting cystic fibrosis lungs promote mechanical

toughness by adjusting polysaccharide production. *NPJ Biofilms Microbiomes.* 3:1.

18. Stoodley, P., R. Cargo, …, I. Klapper. 2002. Biofilm material properties as related to shear-induced deformation and detachment phenomena. *J. Ind. Microbiol. Biotechnol.* 29:361–367.
19. Körstgens, V., H. C. Flemming, …, W. Borchard. 2001. Uniaxial compression measurement device for investigation of the mechanical stability of biofilms. *J. Microbiol. Methods.* 46:9–17.
20. Lieleg, O., M. Caldara, …, K. Ribbeck. 2011. Mechanical robustness of *Pseudomonas aeruginosa* biofilms. *Soft Matter.* 7:3307–3314.
21. Tabata, Y., and Y. Ikada. 1988. Effect of the size and surface charge of polymer microspheres on their phagocytosis by macrophage. *Biomaterials.* 9:356–362.
22. Evans, E., A. Leung, and D. Zhelev. 1993. Synchrony of cell spreading and contraction force as phagocytes engulf large pathogens. *J. Cell Biol.* 122:1295–1300.
23. Jeong, B., J.-S. Park, …, S. Hong. 2007. Direct measurement of the force generated by a single macrophage. *J. Korean Phys. Soc.* 50:313–319.
24. Mercer, F., S. H. Ng, …, P. J. Johnson. 2018. Neutrophils kill the parasite Trichomonas vaginalis using trogocytosis. *PLoS Biol.* 16:e2003885.
25. Li, K. J., C. H. Wu, …, S. C. Hsieh. 2016. Membrane transfer from mononuclear cells to polymorphonuclear neutrophils transduces cell survival and activation signals in the recipient cells via anti-extrinsic apoptotic and MAP kinase signaling pathways. *PLoS One.* 11:e0156262.
26. Valgardsdottir, R., I. Cattaneo, …, J. Golay. 2017. Human neutrophils mediate trogocytosis rather than phagocytosis of CLL B cells opsonized with anti-CD20 antibodies. *Blood.* 129:2636–2644.
27. Taylor, R. P., and M. A. Lindorfer. 2015. Fcγ-receptor-mediated trogocytosis impacts mAb-based therapies: historical precedence and recent developments. *Blood.* 125:762–766.
28. Matlung, H. L., L. Babes, …, T. K. van den Berg. 2018. Neutrophils kill antibody-opsonized cancer cells by trogoptosis. *Cell Rep.* 23:3946–3959.e6.
29. Clarke, M., U. Engel, …, G. Gerisch. 2010. Curvature recognition and force generation in phagocytosis. *BMC Biol.* 8:154.
30. Marion, S., C. Laurent, and N. Guillén. 2005. Signalization and cytoskeleton activity through myosin IB during the early steps of phagocytosis in Entamoeba histolytica: a proteomic approach. *Cell. Microbiol.* 7:1504–1518.
31. Beningo, K. A., and Y. L. Wang. 2002. Fc-receptor-mediated phagocytosis is regulated by mechanical properties of the target. *J. Cell Sci.* 115:849–856.
32. Jensen, P. Ø., T. Bjarnsholt, …, N. Høiby. 2007. Rapid necrotic killing of polymorphonuclear leukocytes is caused by quorum-sensing-controlled production of rhamnolipid by *Pseudomonas aeruginosa*. *Microbiology.* 153:1329–1338.
33. Allen, L., D. H. Dockrell, …, M. K. Whyte. 2005. Pyocyanin production by *Pseudomonas aeruginosa* induces neutrophil apoptosis and impairs neutrophil-mediated host defenses in vivo. *J. Immunol.* 174:3643–3649.
34. Schmitt, A., P. Rödel, …, J. Engert. 2015. Calcium alginate gels as stem cell matrix-making paracrine stem cell activity available for enhanced healing after surgery. *PLoS One.* 10:e0118937.
35. Cereceres, S., Z. Lan, …, E. Cosgriff-Hernandez. 2019. Bactericidal activity of 3D-printed hydrogel dressing loaded with gallium maltolate. *APL Bioeng.* 3:026102.
36. Liang, J.-Z., and R. K. Y. Li. 1999. Brittle–ductile transition in polypropylene filled with glass beads. *Polymer.* 40:3191–3195.
37. Benguigui, L., and P. Ron. 1993. Experimental realization of superelasticity near the percolation threshold. *Phys. Rev. Lett.* 70:2423–2426.
38. Zhang, Z., E. Nadezhina, and K. J. Wilkinson. 2011. Quantifying diffusion in a biofilm of Streptococcus mutans. *Antimicrob. Agents Chemother.* 55:1075–1081.
39. Mark, T., and F. R. D. Quinn. 2014. Neutrophil Methods and Protocols. Humana Press, Totowa, NJ.
40. Alhede, M., K. N. Kragh, …, T. Bjarnsholt. 2011. Phenotypes of non-attached *Pseudomonas aeruginosa* aggregates resemble surface attached biofilm. *PLoS One.* 6:e27943.
41. Hutchison, J. B., C. A. Rodesney, …, V. D. Gordon. 2014. Single-cell control of initial spatial structure in biofilm development using laser trapping. *Langmuir.* 30:4522–4530.
42. Holloway, B. W., and A. F. Morgan. 1986. Genome organization in Pseudomonas. *Annu. Rev. Microbiol.* 40:79–105.
43. Stover, C. K., X. Q. Pham, …, M. V. Olson. 2000. Complete genome sequence of *Pseudomonas aeruginosa* PAO1, an opportunistic pathogen. *Nature.* 406:959–964.
44. Irie, Y., M. Starkey, …, M. R. Parsek. 2010. *Pseudomonas aeruginosa* biofilm matrix polysaccharide Psl is regulated transcriptionally by RpoS and post-transcriptionally by RsmA. *Mol. Microbiol.* 78:158–172.
45. Kragh, K. N., J. B. Hutchison, …, T. Bjarnsholt. 2016. Role of multicellular aggregates in biofilm formation. *MBio.* 7:e00237.
46. Hutchison, J., K. Kaushik, …, V. D. Gordon. 2018. Increased production of the extracellular polysaccharide Psl can give a growth advantage to *Pseudomonas aeruginosa* in low-iron conditions. *bioRxiv* https://doi.org/10.1101/355339.
47. Cooley, B. J., T. W. Thatcher, …, V. D. Gordon. 2013. The extracellular polysaccharide Pel makes the attachment of *P. aeruginosa* to surfaces symmetric and short-ranged. *Soft Matter.* 9:3871–3876.
48. Rodesney, C. A., B. Roman, …, V. D. Gordon. 2017. Mechanosensing of shear by *Pseudomonas aeruginosa* leads to increased levels of the cyclic-di-GMP signal initiating biofilm development. *Proc. Natl. Acad. Sci. USA.* 114:5906–5911.
49. Moe, S. T., K. I. Draget, …, O. Simdsrød. 1992. Temperature dependence of the elastic modulus of alginate gels. *Carbohydr. Polym.* 19:279–284.
50. De Gennes, P. G. 1976. Dynamics of entangled polymer solutions: I. The Rouse model. *Macromolecules.* 9:587–593.
51. Kaklamani, G., D. Cheneler, …, J. Bowen. 2014. Mechanical properties of alginate hydrogels manufactured using external gelation. *J. Mech. Behav. Biomed. Mater.* 36:135–142.
52. Fatin-Rouge, N., K. Starchev, and J. Buffle. 2004. Size effects on diffusion processes within agarose gels. *Biophys. J.* 86:2710–2719.
53. Narayanan, J., J.-Y. Xiong, and X.-Y. Liu. 2006. Determination of agarose gel pore size: absorbance measurements vis a vis other techniques. *J. Phys. Conf. Ser.* 28:83–86.
54. Pluen, A., P. A. Netti, …, D. A. Berk. 1999. Diffusion of macromolecules in agarose gels: comparison of linear and globular configurations. *Biophys. J.* 77:542–552.
55. Li, R. H., D. H. Altreuter, and F. T. Gentile. 1996. Transport characterization of hydrogel matrices for cell encapsulation. *Biotechnol. Bioeng.* 50:365–373.
56. Klein, J., J. Stock, and K.-D. Vorlop. 1983. Pore size and properties of spherical Ca-alginate biocatalysts. *Eur. J. Appl. Microbiol. Biotechnol.* 18:86–91.
57. Choi, N. W., M. Cabodi, …, A. D. Stroock. 2007. Microfluidic scaffolds for tissue engineering. *Nat. Mater.* 6:908–915.
58. Hentzer, M., G. M. Teitzel, …, M. R. Parsek. 2001. Alginate overproduction affects *Pseudomonas aeruginosa* biofilm structure and function. *J. Bacteriol.* 183:5395–5401.
59. Ryder, C., M. Byrd, and D. J. Wozniak. 2007. Role of polysaccharides in *Pseudomonas aeruginosa* biofilm development. *Curr. Opin. Microbiol.* 10:644–648.
60. Franklin, M. J., D. E. Nivens, …, P. L. Howell. 2011. Biosynthesis of the *Pseudomonas aeruginosa* extracellular polysaccharides, alginate, pel, and Psl. *Front. Microbiol.* 2:167.

61. Kastl, L., D. Sasse, …, P. Rivera Gil. 2013. Multiple internalization pathways of polyelectrolyte multilayer capsules into mammalian cells. *ACS Nano.* 7:6605–6618.

62. Galkina, S. I., J. G. Molotkovsky, …, G. F. Sud'ina. 2005. Scanning electron microscopy study of neutrophil membrane tubulovesicular extensions (cytonemes) and their role in anchoring, aggregation and phagocytosis. The effect of nitric oxide. *Exp. Cell Res.* 304:620–629.

63. Trivedi, R. R., J. A. Crooks, …, D. B. Weibel. 2018. Mechanical genomic studies reveal the role of d-alanine metabolism in *Pseudomonas aeruginosa* cell stiffness. *MBio.* 9:e01340-18.

64. Aggarwal, S., E. H. Poppele, and R. M. Hozalski. 2010. Development and testing of a novel microcantilever technique for measuring the cohesive strength of intact biofilms. *Biotechnol. Bioeng.* 105:924–934.

65. Poppele, E. H., and R. M. Hozalski. 2003. Micro-cantilever method for measuring the tensile strength of biofilms and microbial flocs. *J. Microbiol. Methods.* 55:607–615.

66. Herant, M., V. Heinrich, and M. Dembo. 2005. Mechanics of neutrophil phagocytosis: behavior of the cortical tension. *J. Cell Sci.* 118:1789–1797.

67. Sridharan, R., B. Cavanagh, …, F. J. O'Brien. 2019. Material stiffness influences the polarization state, function and migration mode of macrophages. *Acta Biomater.* 89:47–59.

68. Blakney, A. K., M. D. Swartzlander, and S. J. Bryant. 2012. The effects of substrate stiffness on the in vitro activation of macrophages and in vivo host response to poly(ethylene glycol)-based hydrogels. *J. Biomed. Mater. Res. A.* 100:1375–1386.

69. Irwin, E. F., K. Saha, …, K. E. Healy. 2008. Modulus-dependent macrophage adhesion and behavior. *J. Biomater. Sci. Polym. Ed.* 19:1363–1382.

70. Anselmo, A. C., and S. Mitragotri. 2017. Impact of particle elasticity on particle-based drug delivery systems. *Adv. Drug Deliv. Rev.* 108:51–67.

71. Waldmannová, E., V. Caisová, …, J. Ženka. 2016. The use of Zymosan A and bacteria anchored to tumor cells for effective cancer immunotherapy: B16-F10 murine melanoma model. *Int. Immunopharmacol.* 39:295–306.

72. Lee, C. Y., G. R. Thompson, III, …, V. Heinrich. 2015. Coccidioides endospores and spherules draw strong chemotactic, adhesive, and phagocytic responses by individual human neutrophils. *PLoS One.* 10:e0129522.

73. Pier, G. B. 2012. The challenges and promises of new therapies for cystic fibrosis. *J. Exp. Med.* 209:1235–1239.

74. Galli, F., A. Battistoni, …, G. Cabrini; Working Group on Inflammation in Cystic Fibrosis. 2012. Oxidative stress and antioxidant therapy in cystic fibrosis. *Biochim. Biophys. Acta.* 1822:690–713.

Biophysical Journal, Volume *117*

Supplemental Information

Assaying How Phagocytic Success Depends on the Elasticity of a Large Target Structure

Megan Davis-Fields, Layla A. Bakhtiari, Ziyang Lan, Kristin N. Kovach, Liyun Wang, Elizabeth M. Cosgriff-Hernandez, and Vernita D. Gordon

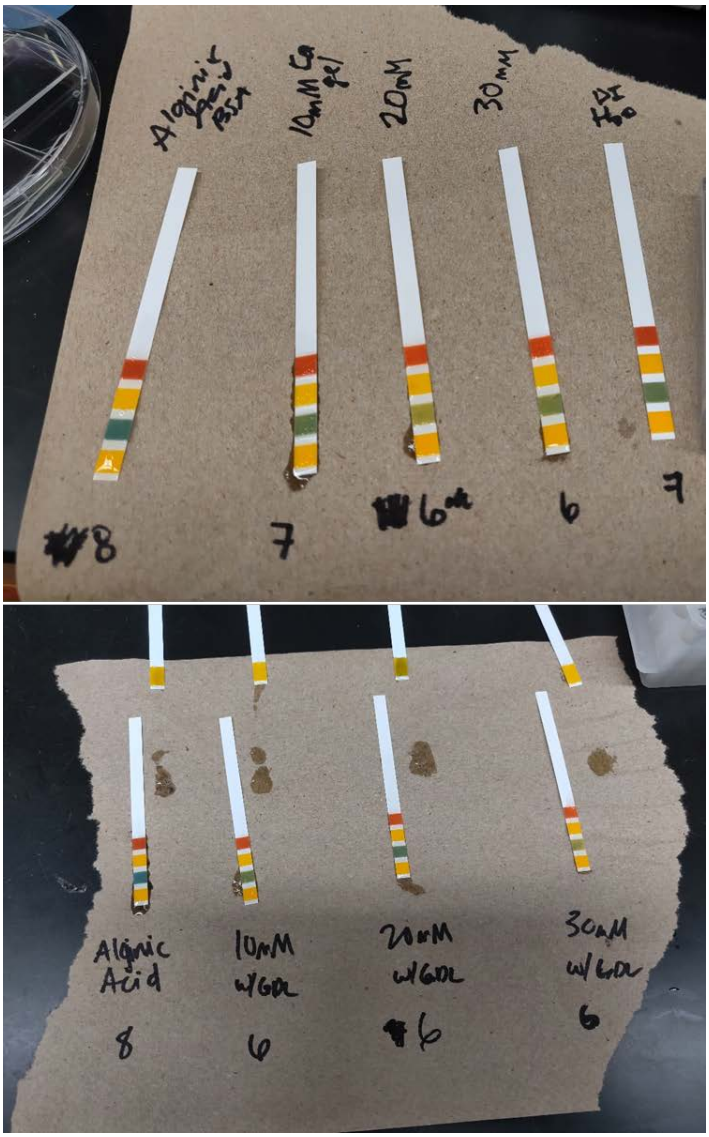

Figure S1. Images of pH test strips showing the change in pH during alginate gel fabrication. The initial alginic acid solution has a pH of 8 and upon the introduction of $CaCO_3$ and GDL the pH reduces to 6 or 7 for gels made with 10mM calcium, and a pH of 6 for gels made with 20mM or 30mM calcium.

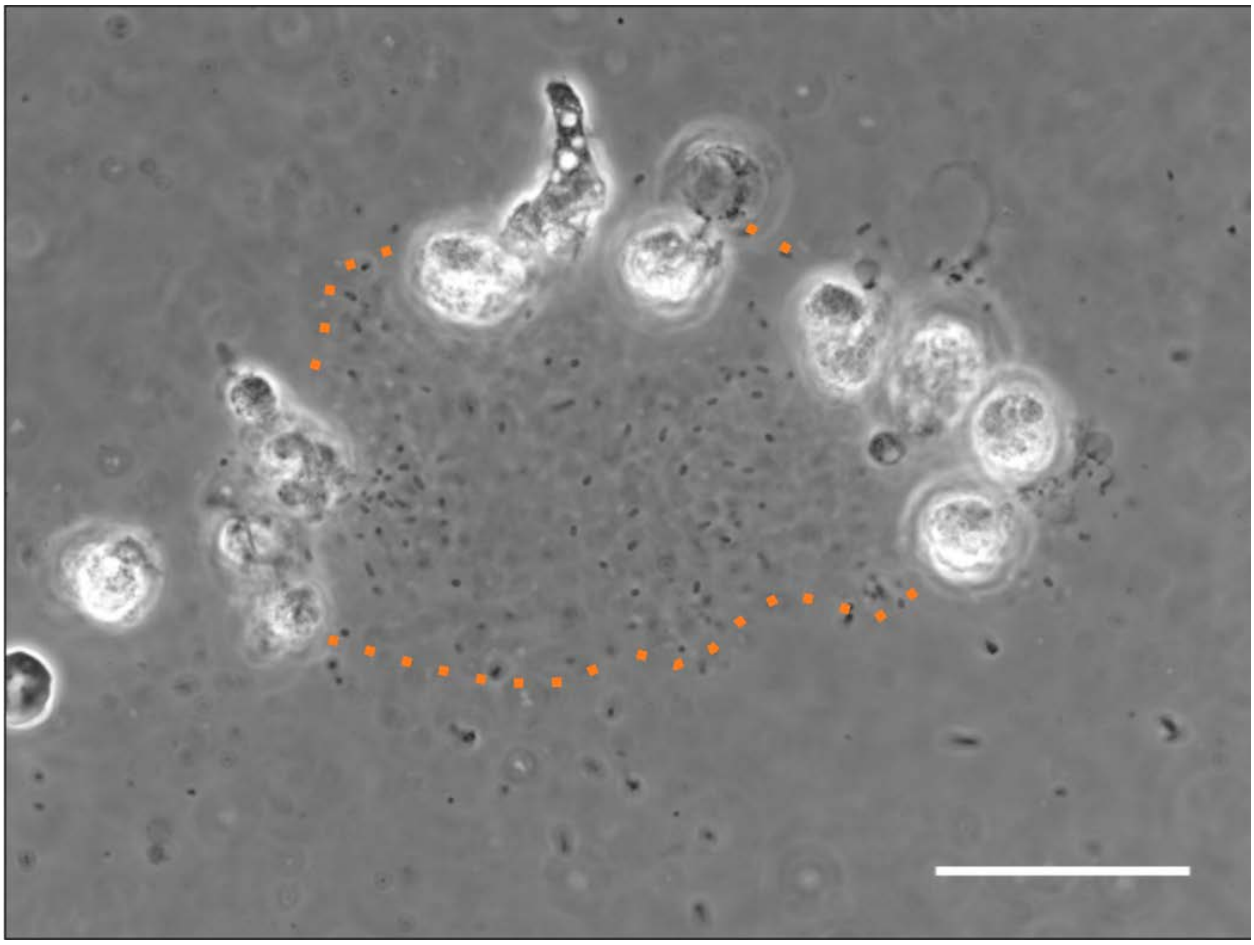

Figure S2. Still frame from neutrophil-biofilm interaction timelapse microscopy video (Supplementary Movie 1). Here the biofilm aggregate is outlined in orange for clarity. The biofilm polymer-protein matrix is not visible by phase contrast microscopy, however aggregates can be recognized as regions that are densely packed with bound bacterial cells that show neither active nor passive motility. Scalebar shown is 30 μm.

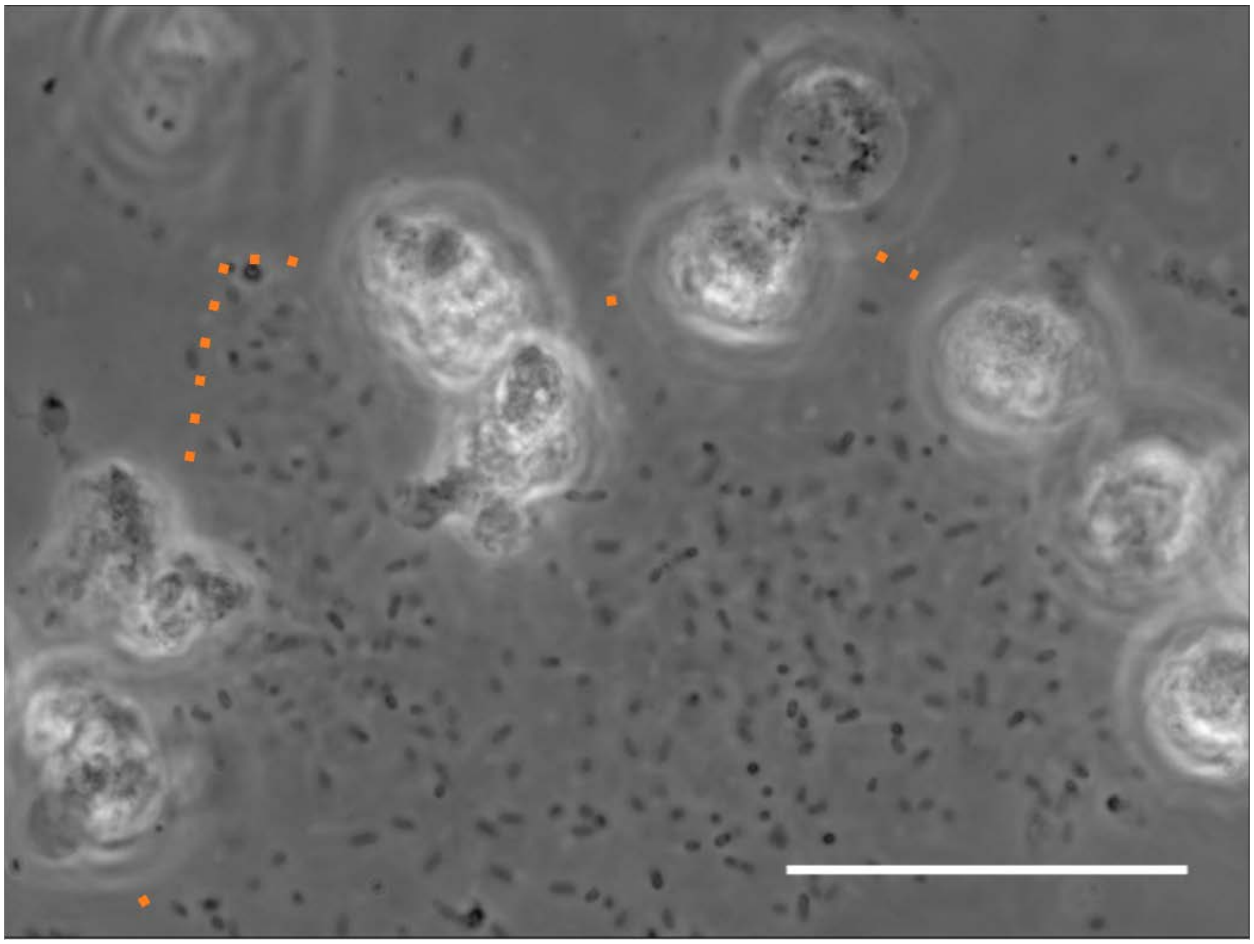

Figure S3. Still frame from neutrophil-biofilm interaction timelapse microscopy video (Supplementary Movie 2). Here the biofilm aggregate is outlined in orange for clarity. The biofilm polymer-protein matrix is not visible by phase contrast microscopy, however aggregates can be recognized as regions that are densely packed with bound bacterial cells that show neither active nor passive motility. Scalebar shown is 30 μm.

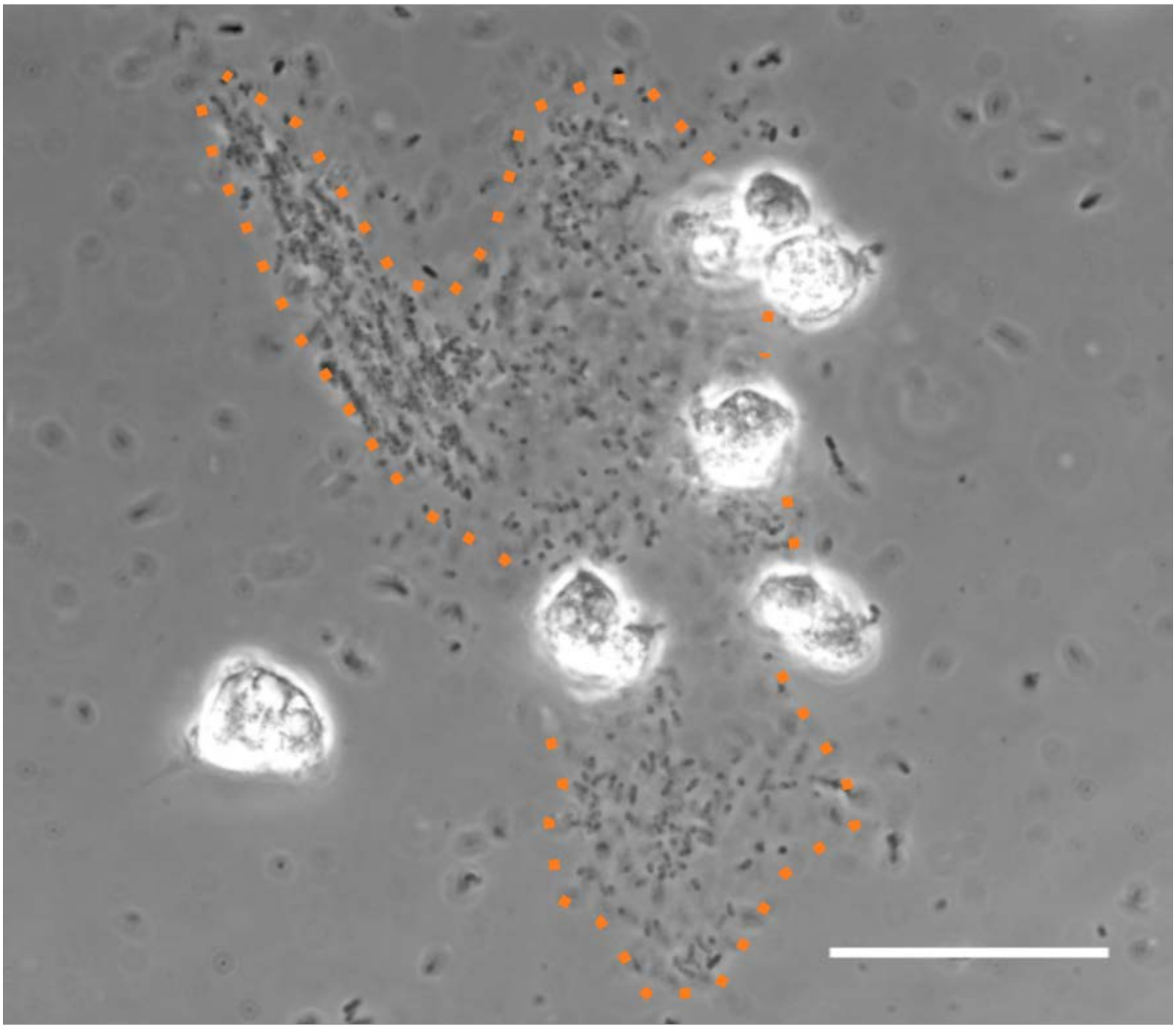

Figure S4. Still frame from neutrophil-biofilm interaction timelapse microscopy video (Supplementary Movie 3). Here the biofilm aggregate is outlined in orange for clarity. The biofilm polymer-protein matrix is not visible by phase contrast microscopy, however aggregates can be recognized as regions that are densely packed with bound bacterial cells that show neither active nor passive motility. Scalebar shown is 30 μm.

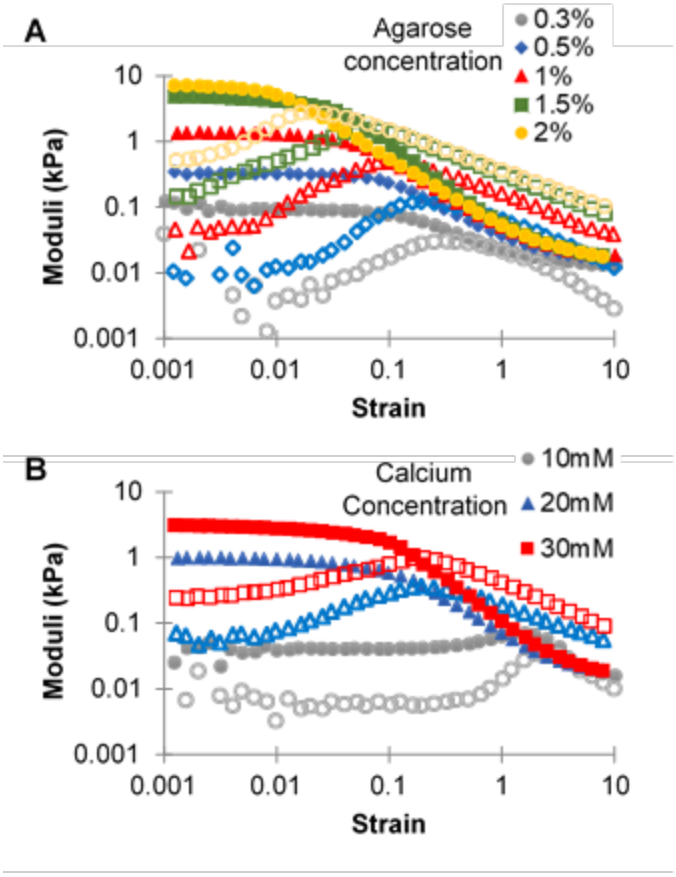

Figure S5. Representative strain sweeps for (A) agarose and (B) alginate gels, all from the same day of measurement. These gels contained fluorescent polystyrene beads and BSA at the concentrations used for engulfment tests. Frequency sweeps were done at 1% strain and strain sweeps were done at 3.14 radians/s. The elastic moduli (G') are shown with solid symbols and the viscous moduli (G'') are shown with hollow symbols of corresponding shape and color.

Supplementary Movie 1. This phase contrast micrograph movie shows neutrophils interacting with and attacking biofilm-like aggregates of bacteria at 8 times real speed. Aggregates can be recognized as the bacteria-dense regions that exclude neutrophils. Bacteria in aggregates show no active motility, such as swimming, and no passive mobility, as in Brownian motion. This is not the case for bacteria outside of aggregates, most of which are actively moving and all of which are subject to Brownian motion. Aggregated bacteria are bound together in a biofilm-like matrix of polymer and protein which is not visible under phase contrast microscopy. Scalebar shown is 30 μm.

Supplementary Movie 2. This phase contrast micrograph movie shows neutrophils interacting with and attacking biofilm-like aggregates of bacteria at 8 times real speed. Aggregates can be recognized as the bacteria-dense regions that exclude neutrophils. Bacteria in aggregates show no active motility, such as swimming, and no passive mobility, as in Brownian motion. This is not the case for bacteria outside of aggregates, most of which are actively moving and all

of which are subject to Brownian motion. Aggregated bacteria are bound together in a biofilm-like matrix of polymer and protein which is not visible under phase contrast microscopy. Scalebar shown is 30 μm.

Supplementary Movie 3. This phase contrast micrograph movie shows neutrophils interacting with and attacking biofilm-like aggregates of bacteria at 8 times real speed. Aggregates can be recognized as the bacteria-dense regions that exclude neutrophils. Bacteria in aggregates show no active motility, such as swimming, and no passive mobility, as in Brownian motion. This is not the case for bacteria outside of aggregates, most of which are actively moving and all of which are subject to Brownian motion. Aggregated bacteria are bound together in a biofilm-like matrix of polymer and protein which is not visible under phase contrast microscopy. Scalebar shown is 30 μm.

Supplementary Movie 4. Phase-contrast microscopy focal scan along the height of a biofilm aggregate and neutrophils (Supplementary Movie 2), showing the three-dimensional structure. Native video playback is set at 3 frames per second. Scalebar shown is 30 μm.

Supplementary Movie 5. Phase-contrast microscopy focal scan along the height of a biofilm aggregate and neutrophils (Supplementary Movie 3), showing the three-dimensional structure. Native video playback is set at 3 frames per second. Scalebar shown is 30 μm.

Supplementary Movie 6. 0.3% agarose immediately after the addition of fluorescent 200nm beads. The gel region (left) excludes the beads after initial introduction. The first frame of the movie file is transmitted light, while the second frame is a fluorescence image of the same field of view.

Supplementary Movie 7. 0.3% agarose 40 minutes after the addition of fluorescent 200nm beads. The gel region (left) continues to exclude the beads, suggesting the pore size of the gel is less than 200nm. The first frame of the movie file is transmitted light, while the second frame is a fluorescence image of the same field of view.

Supplementary Movie 8. Alginate made with 20 mM calcium immediately after the addition of fluorescent 200nm beads. The gel region is on the left of the image.

Supplementary Movie 9. Alginate made with 20 mM calcium 10 minutes after the addition of fluorescent 200nm beads. The gel region is on the left of the image and continues to exclude the beads, suggesting the pore size of the gel is less than 200nm.

Supplementary Movie 10. Alginate made with 30 mM calcium immediately after the addition of fluorescent 200nm beads. The gel region is on the left of the image.

Supplementary Movie 11. Alginate made with 30 mM calcium 10 minutes after the addition of fluorescent 200nm beads. The gel region is on the left of the image and continues to exclude the beads, suggesting the pore size of the gel is less than 200nm.

Supplementary Movie 12. 0.3% agarose immediately after the addition of dyed dextran with hydrodynamic radius 35nm. The gel already contains a great deal of dextran.

Supplementary Movie 13. Alginate made with 20 mM calcium immediately after the addition of dyed dextran with hydrodynamic radius 35nm. A small amount of dextran has entered the gel.

Supplementary Movie 14. Alginate made with 20 mM calcium 10 minutes after the addition of dyed dextran with hydrodynamic radius 35nm. The gel now contains more dextran than it did at t=0.

Supplementary Movie 15. Alginate made with 30 mM calcium immediately after the addition of dyed dextran with hydrodynamic radius 35nm. Little to no dextran has entered the gel.

Supplementary Movie 16. Alginate made with 30 mM calcium 10 minutes after the addition of dyed dextran. The amount of dextran in the gel has increased slightly or not at all since t=0.

Supplementary Movie 17. Timelapse microscopy video observing the interaction of neutrophils (on the right) with alginate gel made using 20mM of $CaCO_3$ (on the left). The neutrophils are attracted by the target and crawl along the boundary, but do not penetrate the gel. Video is displayed at 37 frames per second, and was acquired at 1 frame per minute. 450 frames were taken over the course of 450 seconds (7.5 mins). Scalebar is 60 μm.

Supplementary Movie 18. Timelapse microscopy video observing the interaction of neutrophils (on the right) with alginate gel made using 20mM of $CaCO_3$ (on the left). The neutrophils are attracted by the target and crawl along the boundary, but do not penetrate the gel. Video is displayed at 37 frames per second, and was acquired at 1 frame per minute. 551 frames were taken over the course of 551 seconds (9.18 mins). Scalebar is 60 μm.

Supplementary Movie 19. Timelapse microscopy video observing the interaction of neutrophils (on the right) with alginate gel made using 30mM of $CaCO_3$ (on the left). The neutrophils are attracted by the target and crawl along the boundary, but do not penetrate the gel. Video is displayed at 37 frames per second, and was acquired at 1 frame per minute. 450 frames were taken over the course of 450 seconds (7.5 mins). Scalebar is 60 μm.

Supplementary Movie 20. Timelapse microscopy video observing the interaction of neutrophils (on the right) with a 0.5% agarose gel. Agarose gel cannot directly be visualized by phase contrast microscopy, however polystyrene beads embedded within the gel provide visualization

of the gel region (on left). The neutrophils are attracted by the target and crawl along the boundary, but do not penetrate the gel. Video is displayed at 37 frames per second, and was acquired at 1 frame per minute. 421 frames were taken over the course of 421 seconds (7 mins). Scalebar is 60 μm.

Supplementary Movie 21. Timelapse microscopy video observing the interaction of neutrophils (on the right) with a 0.3% agarose gel. Agarose gel cannot directly be visualized by phase contrast microscopy, however polystyrene beads embedded within the gel provide visualization of the gel region (on left). The neutrophils are attracted by the target and crawl along the boundary, but do not penetrate the gel. Video is displayed at 37 frames per second, and was acquired at 1 frame per minute. 2000 frames were taken over the course of 2000 seconds (33.33 mins). Scalebar is 60 μm.

Supplementary Movie 22. Timelapse microscopy video observing the interaction of neutrophils (on the right) with a 0.3% agarose gel. Agarose gel cannot directly be visualized by phase contrast microscopy, however polystyrene beads embedded within the gel provide visualization of the gel region (on left). The neutrophils are attracted by the target and crawl along the boundary, but do not penetrate the gel. Video is displayed at 37 frames per second, and was acquired at 1 frame per minute. 2000 frames were taken over the course of 2000 seconds (33.33 mins). Scalebar is 60 μm.

Supplementary Movie 23. Confocal z-stack of 0.3% agarose gel with neutrophils on top, immediately after the addition of neutrophils to the gel. Fluorescence signal is false-colored magenta and transmitted light is false-colored blue. The neutrophils settled onto the top surface of the gel. Scalebar is 60 μm. Native video playback is set at 10 FPS.

Supplementary Movie 24. Confocal z-stack of 0.3% agarose gel with neutrophils on top, 60 minutes after the addition of neutrophils to the gel. Fluorescence signal is false-colored magenta and transmitted light is false-colored blue. Neutrophils remain localized within a similar z slice as the initial time point (Supplementary Movie 23) and do not appear to have penetrated into the gel after one hour of contact with the surface. Scalebar is 60 μm. Native video playback is set at 10 FPS.

Supplementary Movie 25. Confocal z-stack of 0.3% agarose gel with neutrophils on top, 120 minutes after the addition of neutrophils to the gel. Fluorescence signal is false colored magenta and transmitted light is false colored blue. Neutrophils remain localized within a similar z slice as the initial time point (Supplementary Movie 23) and do not appear to have penetrated into the gel after two hours of contact with the surface. Scalebar is 60 μm. Native video playback is set at 10 FPS.